Supplementary information

Full range physiological mass transport control in 3D tissue cultures

Yu-Hsiang Hsu[a,f], Monica L. Moya[a,f], Parinaz Abiri[a], Christopher C.W. Hughes [a,b,f†], Steven C. George [a,c,d,f†], Abraham P. Lee[a,e†*]

Affiliations:

[a] Departments of Biomedical Engineering, University of California, Irvine, USA

[b] Molecular Biology and Biochemistry, University of California, Irvine, USA

[c] Chemical Engineering and Materials Science, University of California, Irvine, USA

[d] Medicine, University of California, Irvine, USA

[e] Mechanical and Aerospace Engineering, University of California, Irvine, USA

[f] Edwards Lifesciences Center for Advanced Cardiovascular Technology, University of California, Irvine, USA

[†]These authors contributed equally to this work

*Correspondence to: aplee@uci.edu

Design of microfluidic long side channel

Considering a pressure driven Poiseuille flow in a long, straight and rigid channel, the volume flow rate Q is determined by the ratio of the driving pressure difference ΔP and the hydraulic resistance R (S1),

$$Q = \frac{\Delta P}{R}. \tag{S1}$$

With a given driving pressure difference ΔP, the volume flow rate Q is based on the hydraulic resistance R. The higher the hydraulic resistance R, the lower the volume flow rate Q. Applying this fundamental fluidic dynamics into the present microfluidic platform, this equation provides two design freedoms. First, it states that a relative constant pressure drop can be maintained by the two media reservoirs with a very low volume flow rate Q, which can be achieved by having a large hydraulic resistance R. Second, the volume flow rate and fluidic shear stress of the side channel next to the communication pores can be controlled by modifying the hydraulic resistance R.

To create a high hydraulic resistance, the hydraulic resistance of a straight channel with rectangular R_{rec} and square R_{sq} cross-sections were considered. They are (S2)

$$R_{rec} = \frac{12}{(w/h) - 0.63} \frac{\eta L}{h^4} \text{ for } w > h \tag{S2}$$

and $$R_{sq} = 28.47\frac{\eta L}{h^4}, \quad \text{(S3)}$$

where w, h and L are the width, height, and length of the straight channel, and η is the fluidic viscosity. Since the thickness of the microfluidic channel is fixed to 100 μm, the hydraulic resistance of a rectangular channel was determined by the w/h ratio and length L. Equation (S2) clearly shows that the highest hydraulic resistance of a rectangular channel is w/h close to 1, which is close to a square channel. Thus, the cross-section of the long side channel was chosen to be square to have the highest achievable hydraulic resistance. Further, to substantially increase the hydraulic resistance of the side channel, the length L was increase to be 510 to 780 mm long. This design offered an additional degree of freedom. By routing the long side channel around the microchamber, different pattern and magnitude of pressure gradient and physiological conditions was created.

The influence of the geometrical cross-section to the hydraulic resistance can also be represented by diving Eq. (S3) by Eq. (S2),

$$\frac{R_{sq}}{R_{rec}} = 2.3725[(w/h) - 0.63]. \quad \text{(S4)}$$

Assuming that the width w is 5 times larger than the height h, $w/h = 5$, the R_{sq}/R_{rec} ratio becomes 10.37. It demonstrated that the hydraulic resistance of a rectangular channel can be 10 times higher than a rectangular channel. It also shows that the volume flow rate Q can be easily slowed down to more than 10 times. In the present study, the w/h ratio of side channels next to microchamber was controlled to have a higher flow rate compared to the rate of created mass transport for mimicking normal in vivo oxygen levels in the long side channel. The calculated velocity ratios V_R of platforms shown in Figs. 3A to 3D were 9, 31, 207, and 13,000, respectively. The velocity ratios V_R of the ones shown in Figs. S2 to S5 with 16 communication pores were 9.5, 68, 405, and 9,450, respectively.

Calculation of Péclet number

We quantitatively expressed the relative magnitude of convection to diffusion using the Peclét number (Pe). Pe is defined as the ratio of mass transport by convection to that of diffusion using Eq. (S4).

$$\mathrm{Pe} = \frac{V_a L}{D_{AB}}, \quad \text{(S4)}$$

where V_a is the averaged velocity in the microtissue chamber, L is the characteristic length of the microtissue chamber, and D_{AB} is the molecular diffusivity of the nutrition A (eg., VEGF and oxygen) in medium B (eg., tissue). The diffusion coefficient was 7×10^{-11} m^2/s, and the characteristic length was the width of the microtissue chamber (1mm).

The design of microfluidic jumper

To facilitate loading sequence and post investigation, the long side channel was broken up into two segments on each side of the microchamber connected by a microfluidic "jumper" – a silicone tube that interconnects channel inlets. The "jumper" served three functions: First, the breakup of the long side channel allows minimal shear stress exerted on the fibrin gel while introducing media into the side channels. Second, different physiological environments could be maintained during the development of microvascular network when the jumper was installed. Third, this jumper could be removed and different pressures and nutrition compositions could be applied separately in each channel for post investigation of the developed microvasculature and microtissues. For example, one side channel can simulate arteriole and the other can simulate venule. Figures S1A, S1B, S1C show jumpers designed for microplatforms show in Figs. 3A, 3C and 3D, respectively.

Results of microplatforms with 8 and 16 communication pores

Figures S2A, S3A, S4A and S5A show finite element simulated pressure field of the microplatforms with 16 communication pores (eight on each side) with identical configurations shown in Figs. 2A, 2B, 2C, and 2D, respectively. Figures S3B and S4B show the distribution of interstitial flow (black lines) induced by dominated convective flow at high Pe number. Figure S4B shows a relative lower pressure gradient for creating an intermediate condition by using a shorter microchannel between two sides of the microtissue chamber. The near zero pressure gradient show in Fig. S5b demonstrated that a diffusion dominated physiological environment is created. The figures shown in Figs. S2C, S3C, S4C, and S5C are two time lapses images of flowing fluorescent dextran into microtissue chambers by the mass transported controlled by the long microchannel. The corresponding simulated results are also shown in Figs. S2D, S3D, S4D, and S5D, respectively. Figures S6 and S7 summarized the capillary morphogenesis developed by using microplatfroms with 8 and 16 communication pores, respectively. The biphasic effect of vasculogenesis with respect to Pe number is clearly evidanced.

Supplementary figures:

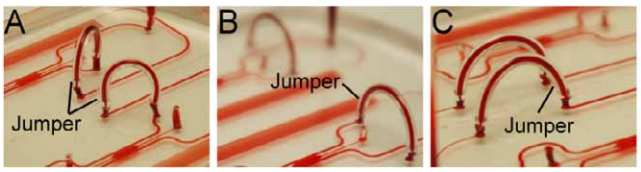

Fig. S1. (A-C) are microfluidic jumpers designed for microplatform shown in Figs. 2a, 2c and 2d.

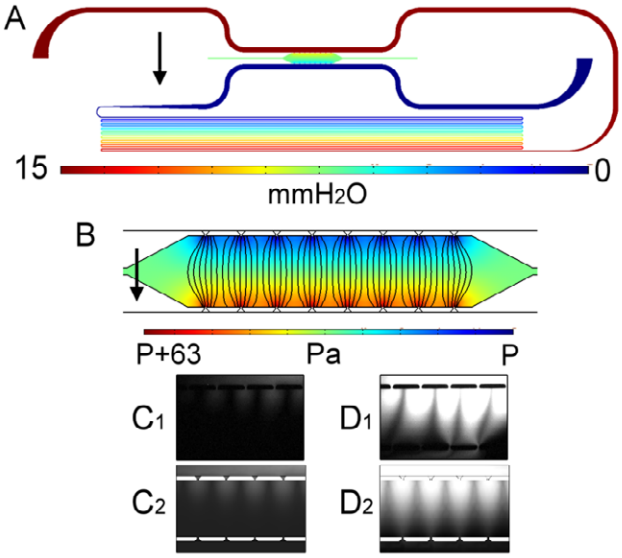

Fig. S2. (A) Microfluidic configuration and the pressure field of the convection-dominated microplatform with 16 communication pores for generating high interstitial flow in transverse direction at Pe > 10. (B) A higher magnification image of simulated pressure field and pattern of interstitial flow (black lines). The experimental and concentration patterns of dextran flowing into the microchamber at time 0 (C_1) and 90 s (C_2) later. The corresponding simulation results at time 0 (D_1) and 60 s (D_2) later.

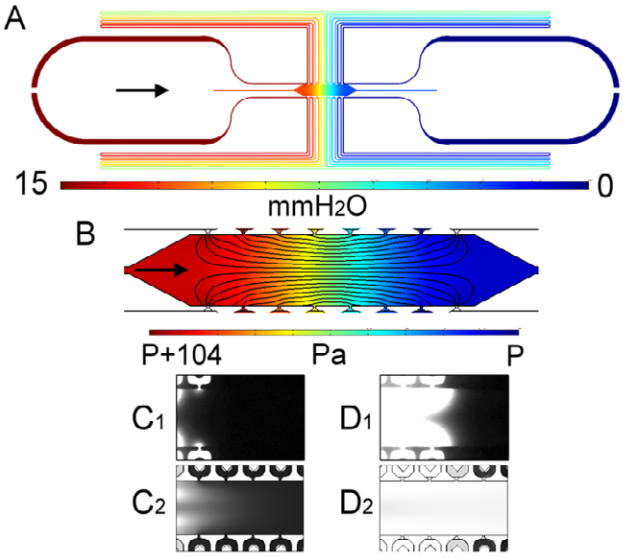

Fig. S3. (A) Microfluidic configuration and the pressure field of the convection-dominated microplatform with 16 communication pores for generating high interstitial flow in longitudinal direction at Pe > 10. (B) A higher magnification image of simulated pressure field and rotated pattern of interstitial flow (black lines). The experimental and concentration patterns of dextran flowing into the microchamber at time 0 (C_1) and 20 min. (C_2) later. The simulation results at time 0 (D_1) and 21 min. (D_2) later.

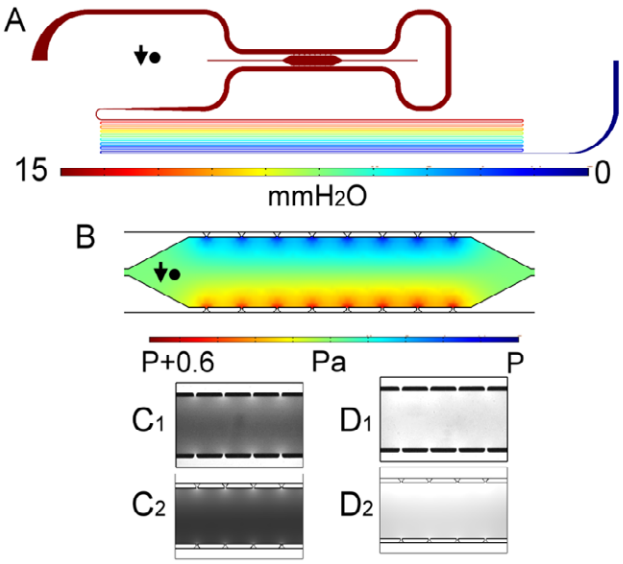

Fig. S4. (A) Microfluidic configuration and the pressure field in which convection and diffusion mass transport are of similar magnitude (Pe ~ 1, 16 communication pores). (B) A higher magnification image of simulated pressure field. The experimental and concentration patterns of dextran flowing into the microchamber at time 0 (C_1) and 4 hours (C_2) later. The corresponding simulation results at time 0 (D_1) and 4 hours (D_2) later.

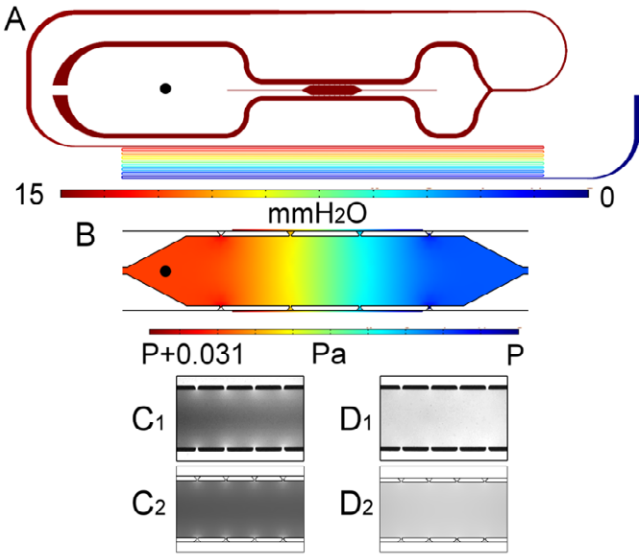

Fig. S5. (A) Microfluidic configuration and the pressure field of the diffusion dominated microplatform with 16 communication pores generating hypoxia at Pe < 0.1. (B) A high magnification image of simulated pressure field, where the transverse pressure gradient is zero, and the longitudinal pressure gradient is near zero. The experimental and concentration patterns of dextran flowing into the microchamber at time 0 (C1) and 2 hours (C1) later. The corresponding simulation results at time 0 (D2) and 2 hours (D2) later.

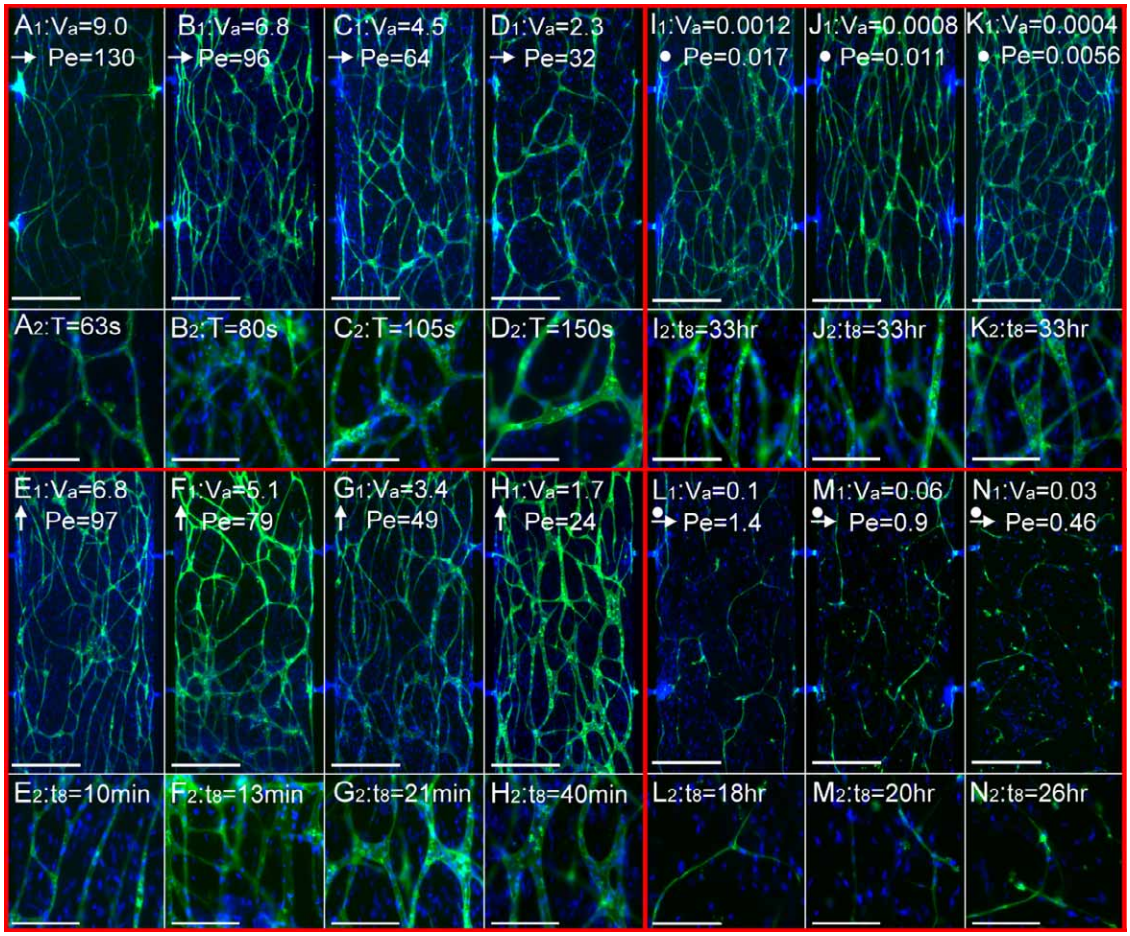

Fig. S6. Micrographs of capillary morphogenesis developed by using microplatfroms with 8 communication pores. (A-D) are capillary morphogenesis of microvasculature developed under transverse interstitial flow at Pe > 10, where V_R=9. (E-H) are capillary morphogenesis of microvasculature developed under longitudinal interstitial flow at Pe > 10, where V_R = 31. (I-K) are capillary morphogenesis of microvasculature induced by hypoxia at Pe < 0.1, where V_R = 13,000. (L-N) are capillary morphogenesis of microvascularture developed at Pe ~ 1 regime, where V_R = 207. Capillaries and nuclei were stained with anti-human CD31 antibody and DAPI. The unit of the average interstitial flow V_a is μm/s. Micrographs with subscript 1 and 2 are taken with 40X and 100X magnification, where scale bars are 500 μm and 200 μm, respectively. Arrows and circles indicate the convective and diffusive mass transport, and the direction and length of arrows are the direction and relative magnitude of introduced interstitial flow.

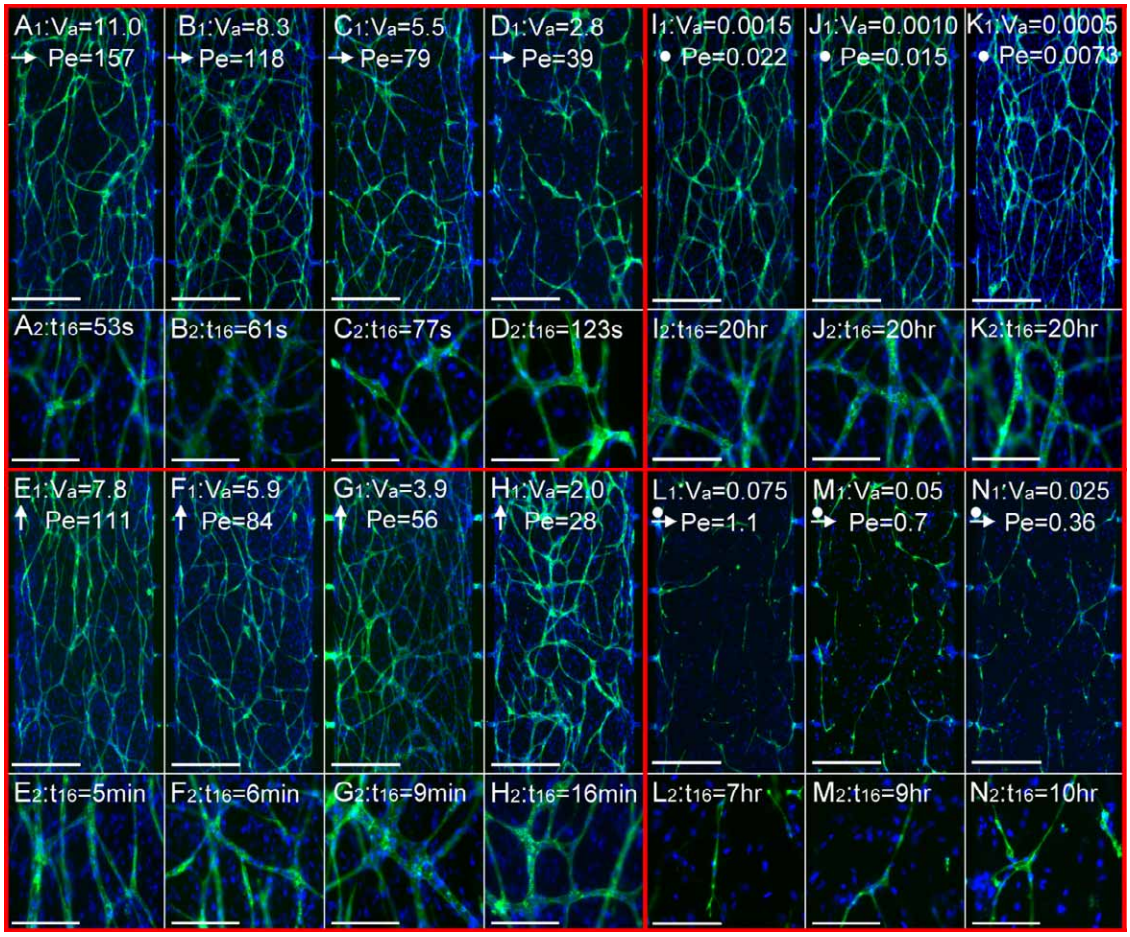

Fig. S7. Micrographs of capillary morphogenesis developed by using microplatfroms with 16 communication pores. (A-D) are capillary morphogenesis of microvasculature developed under transverse interstitial flow at Pe > 10, where V_R = 9.5. (E-H) are capillary morphogenesis of microvasculature developed under longitudinal interstitial flow at Pe > 10, where V_R = 68. (I-K) are capillary morphogenesis of microvasculature induced by hypoxia at Pe < 0.1, where V_R = 9,450. (L-N) are capillary morphogenesis of microvascularture developed at Pe ~ 1 regime, where V_R = 405. Capillaries and nuclei were stained with anti-human CD31 antibody and DAPI. The unit of the average interstitial flow V_a is μm/s. Micrographs with subscript 1 and 2 are taken with 40X and 100X magnification, where scale bars are 500 μm and 200 μm, respectively. Arrows and circles indicate the convective and diffusive mass transport, and the direction and length of arrows are the direction and relative magnitude of introduced interstitial flow.